Hindawi
Shock and Vibration
Volume 2018, Article ID 4217127, 13 pages
https://doi.org/10.1155/2018/4217127

Research Article

Multiple Scattering of P_1 Waves by Arbitrarily Arranged Cavities in Saturated Soils

Miaomiao Sun,[1] **Huajian Fang**,[2,3] **Xiaokang Zheng**,[1] **Ru Zhang**,[1] **Shimin Zhang**,[1] **and Lianying Zhou**[1]

[1]*Zhejiang University City College, Hangzhou, Zhejiang 310015, China*
[2]*Zhejiang Institute of Hydraulics and Estuary, Hangzhou, Zhejiang 310020, China*
[3]*Zhejiang Provincial Key Laboratory of Hydraulics Disaster Prevention and Mitigation, Hangzhou, Zhejiang 310020, China*

Correspondence should be addressed to Miaomiao Sun; sunmm@zucc.edu.cn

Received 6 September 2017; Revised 1 January 2018; Accepted 8 January 2018; Published 7 March 2018

Academic Editor: Tai Thai

Based on Biot's saturated soil wave theory, using wave function expansion method, theoretical solutions of multiple scattering of plain P_1 waves are achieved by rows of cavities as barrier with arbitrarily arranged cavities in saturated soil. Undetermined complex coefficients after wave function expansion are obtained by cavities-soil stress and displacement free boundary conditions. Numerical examples are used to investigate variation of dimensionless displacement amplitude at the back and force of cavities barrier under P_1 wave incident, and it is also discussed that the main parameters influenced isolation effect such as scattering orders, separation of cavities, distances between cavity rows, numbers of cavities, and arrangement of barriers. The results clearly demonstrate optimum design proposals with rows of cavities: with the multiple scattering order increases, the displacement amplitude tends to converge and the deviation caused by subsequent scattering cannot be neglected; it will obtain higher calculation accuracy when the order of scattering is truncated at $m = 4$; it is considered to select $2.5 \le s_p/a_s \le 3.0$ and $2.5 \le h/a_s \le 3.5$, while designing cavity spacing and row-distance, respectively. The isolation properties of elastic waves with rectangular arrangement (counterpoint) are weaker than that with hexagonal arrangement (counterchanged) when the row-distance of barrier is uniform.

1. Introduction

With the accelerated process of urbanization, cities have been expanding continuously. Artificial vibration caused by large-scale construction is increasingly frequent, whether the mechanical vibration during the construction process or the traffic load during running period will do harm to adjacent constructions, underground pipelines, tunnels, and important equipment. It will also affect people's production and life. Therefore, the approach to deal with decreasing artificial vibration and controlling vibration pollution has become one of the most important research topics in soil dynamics.

As a representative discontinuous barrier of vibration isolation, rows of cavities not only can be convenience to construction and supporting, but also are more economical than rows of piles as barrier (Figure 1), because it need not be excavated as empty trench or continuous wall. Therefore it is concerned as an idea measure to be adopted in the vibration pollution control project, especially in saturated soft soil area with high underground water level. As the research basis of rows of cavities as barrier, the problem of refraction and scattering of elastic waves in cylindrical interface has been studied by researchers worldwide [1–4].

Since the calculation of cavities as barrier is usually regarded as the same origin of piles as barrier, many literatures are concentrated on pile rows. Liao and Sangery [5] calculated the passive isolation vibration of solid and hollow piles in far field by introducing acoustical propagation model in 2D fluid media. Kattis et al. [6] numerically solved vibration isolation of one-row piles with 3D frequency domain BEM. Tsai et al. [7] used 3D frequency domain FEM to simulate the block process of Rayleigh waves by one-row pile barrier with various materials in half-space. Xu et al. [8] used complex variable method to investigate the characteristics of elastic wave scattering by arbitrarily shaped cavities in

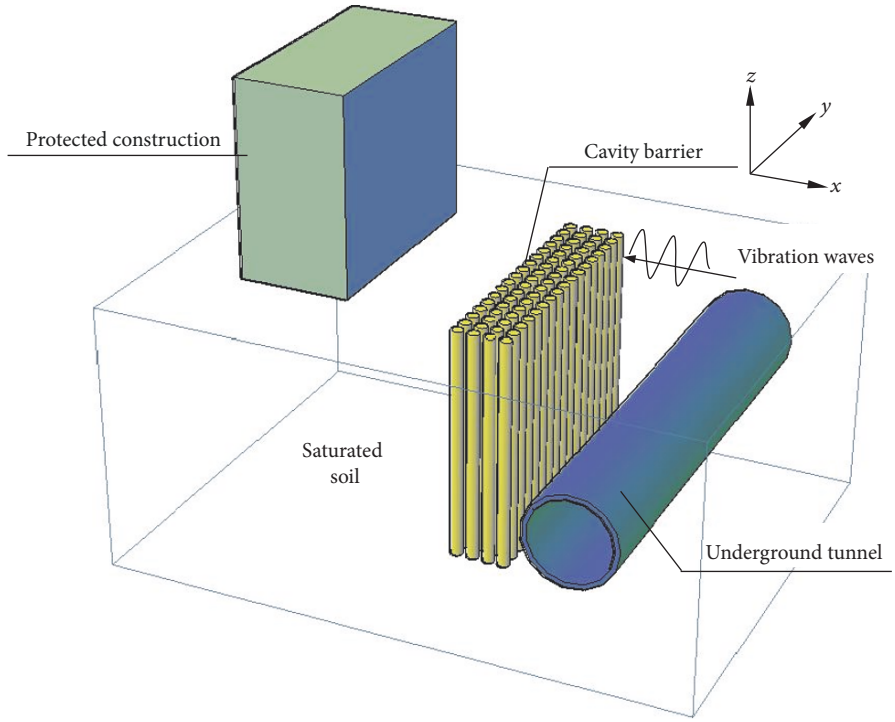

Figure 1: The sketch of artificial isolation vibration by cavities as discontinuous barrier.

saturated soil and gave transient solutions as well. Lu et al. [9] derived the solution of isolation vibration problem of pile rows subjected to high speed moving load, and then they developed a new type of pile rows-linked pile rows. With establishing numerical model by Fourier transformation and BEM, they concluded that the isolation effect of rows-linked piles is better than free-style piles [10]. Recently, Huang and Shi [11–13] regarded discontinuous barrier as periodic structure, and they have obtained attenuation domains range which covers dominant frequencies with various vibrations. They provided a new insight into the analysis and design of pile barriers to block vibrations. Zhang and Lu [14] established a wave domain BEM model for the half-space soil and also considered piles as periodic structure. Carta et al. [15] presented a mathematical model to calculate elastic fluid-filled cylinders subjected to industry-inspired problem. Turan et al. [16] investigated an inclined secant micropile wall positioned as an active vibration barrier with 3D time domain finite element models. On account of its inaccuracy to assume the actual soil as monophasic medium, Cai et al. [17, 18] theoretically solved elastic wave scattering problem by single-row discontinuous barrier in full space using Biot's saturation equation. Thereafter Xu and Xia [19] developed a theoretical method to solve the one-row hollow pile barrier under the P_1 wave incident in saturated soil as well.

Researches specialized in cavities as barrier are stemmed from 1970s. Woods et al. [20] carried out experimental research of cavity rows with holographic method and proposed an evaluation criteria called Amplitude Reduction Coefficient $(1-A_{RC})$ indicating dimensionless isolation effectiveness, which is still used to assess designing requirement so far. Xu et al. [21] used conformal mapping complex variable function method and wave function expansion method to discover the vibration isolation effect by multirow of cylindrical and honeycomb-shaped cavities under plane P and SV wave incident, and results showed that vibration isolation effect would be much better when the number of cavities increases.

On the other hand, isolation vibration is derived from the propagation of elastic waves, which contains multiple scattering and diffraction process. It is usually taken into account in the field of acoustics and electromagnetism. The *multiple scattering* theory can be traced back to the past century, Twersky [22, 23] initiated the study with multiple scattering of infinite cylinders subjected to acoustical and electromagnetic waves in elastic media. An unrecognized backscattered phenomenon occurs, of which the coherent radiative waves propagate through media imbedding several scatterers, such as the thick cloud in the sunshine; incident waves would be scattered multiple times. Considerable peak intensity at the backscattering orientation by homologic backscattered effect is generated, which cannot be neglected in physics and engineering. Sancar and Pao [24] and Sancar and Sachse [25] derived multiple scattering analytical solutions of P waves by two cylindrical cavities in homogeneous isotropic media on the basis of Twesky's work, which provides theoretical ground of ultrasonic nondestructive testing technology. Xia et al. [26, 27] proposed theoretical solutions of body waves' scattering by arbitrarily arranged and shaped discontinuous barriers (solid and hollow piles) in single-phase medium by introducing the multiple scattering method firstly.

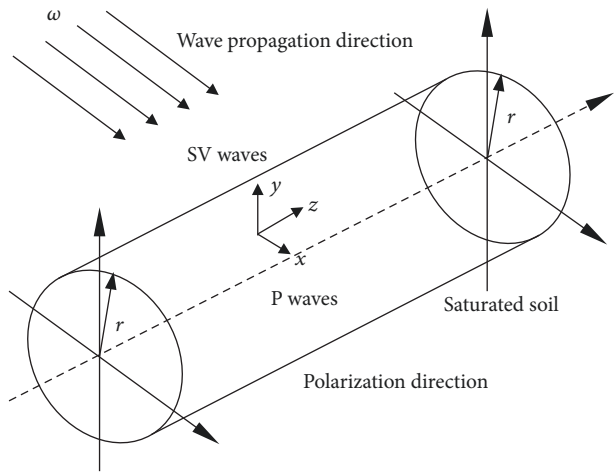

Figure 2: The propagation of elastic waves subjected to a hollow cylinder.

However, most of the studies mentioned above are still aimed at single-phase medium, which does not conform to real physical process of solid-liquid coupling scattering between soil skeleton and fluid in saturated soil. Literatures are rarely focused on elastic waves propagation in a number of arbitrarily arranged and arbitrary radius cavities, and much less attention is paid to coherent scattering law of elastic waves encountering multiple irregular cavities in saturated medium with the point of view of multiple scattering. Therefore, based on Biot's poroelastic theory [28, 29] and multiple scattering method [23], with wave function expansion, this paper proposes the theoretical solution of multiple scattering under plane P_1 wave incident when it confronts with arbitrarily arranged and arbitrary radius cavities in saturated soil. The normalized displacement amplitude behind the cavity barrier is numerically analyzed, which has certain engineering guiding significance for vibration isolation.

2. Methodology

2.1. Theoretical Model. Assuming a hollow cylinder embedded in saturated medium with infinite length (Figure 2), the z-direction of coordinate is along with the length axis of cylinder, and the radius of cross-section is r. A series plain strain waves with frequency of ω are incident with x-axis from the saturated medium. Therefore there exist P_1, P_2, and SV waves' scattering as depicted in Figure 2. Multiple scattering model for several different radii and arbitrarily arranged heterogeneities under plane wave's incident as mentioned in the literature is used [27]. By replacing heterogeneities with cavities (hole-rows), the model is shown at Figure 3, and the medium around is saturated soil. It is assumed that incident angle of the incident P waves is θ_0; setting a point K as study object at far wave field arbitrarily and cavity O as the initial heterogeneity, a Cartesian rectangular coordinate system x-y with origin O is established which is the centroid of the certain cavity. It is obvious that coordinates of K are r, θ; in the next place, another cavity s is chosen as the object of study in wave field, and the relative coordinates of K point to s are r_s, θ_s; rest can be done as the same manner; for example, the

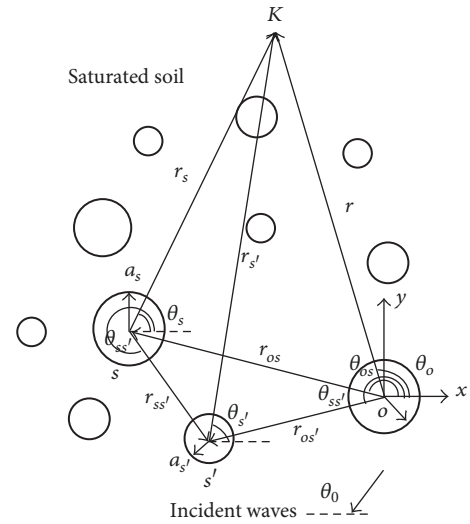

Figure 3: 2D model of plain P_1 waves' multiple scattering by arbitrarily arranged and arbitrary radius cavity barrier in saturated soil.

relative coordinate of K point to s' is $r_{s'}$, $\theta_{s'}$. On the other hand, the relative coordinates of cavity s to cavity o are r_{os}, θ_{os}, the relative coordinates of cavity s' to cavity o are $r_{os'}$, $\theta_{os'}$, and so as the cavity s to s' is $r_{ss'}$, $\theta_{ss'}$ and so on.

The physical process of multiple scattering could be described as follows: an arbitrary subject of scatterer is named as s, which is excited by the incident P_1 waves ${}^s\phi^{\text{inc}}$ initially. A potential function ${}^s\phi_1^{\text{sc}}$ with this scattering of the first order is defined. With the addition to the incident P_1 waves, the total wave field of scatterer s can be expressed as ${}^s\phi = {}^s\phi^{\text{inc}} + {}^s\phi_1^{\text{sc}}$, which satisfies the radiation condition of scatterer s under the specific coordinate system; thus it can be solved by prescribed boundary conditions at the interface. If there are multiple scatterers in this medium, the total wave field is the sum of all the scatters ${}^s\phi_1 = {}^s\phi^{\text{inc}} + \sum_s^{\infty} {}^s\phi_1^{\text{sc}}$. This is usually so-called the single scattering hypothesis. Subsequently, the first order of scattering waves (from the remaining scatterers s' s'', etc.) is the secondary excitation wave to the specific

scatterer s, which performs the second scattering wave field as $\sum_{s'}^{\infty} {}^{s'}\phi_1^{sc}$. The total wave field is ${}^{s}\phi_2 = \sum_{s'}^{\infty} {}^{s'}\phi_1^{sc} + {}^{s}\phi_2^{sc}$ that is also contented with the required boundary conditions. The successive order of scattering mth could be produced in the same way. Making order m approach to infinite and summing up all the scattering wave potentials, ${}^{s}\phi = \sum_{m}^{\infty} {}^{s}\phi_m$ is gained as the total scattering waves of scatterer s finally.

Based on the modified Biot's wave function [30], the influence of inertial additional mass of solid-liquid phase is neglected; it is just considered compression of soil skeleton and the viscous coupling effect of fluid and soil skeleton. As known to all, it gives coupled scattering when it is confronted with incident P waves in saturated medium, which produces three kinds of scattering waves, compressional fast wave P_1, compressional slow wave P_2, and shear wave S. In consideration of incident P_2 wave's rapid attenuation in saturated soil and occupying small quantity energy of elastic waves, the P_2 wave is neglected in propagation of elastic waves induced by artificial vibration, while the effects of wave P_1 are only considered.

The incident P waves' potential function is expanded into a series of Fourier-Bessel series in cylindrical coordinate system such as

$$ {}_{s}^{s}\phi^{\text{inc}} = e^{i\alpha_{1s} r_{0s}(\theta_0 + \theta_{0s})} \sum_{n=-\infty}^{+\infty} J_n(\alpha_{1s} r_s)\, e^{in\varphi_s} e^{-i\omega t}, \tag{1} $$

where the superscript inc of ϕ on the right side defines the incident wave, the subscript s on the left side is soil skeleton, the superscript s on the left side indicates sth cavity, $J_n(\cdot)$ indicates nth-order Bessel function, α_{1s} is the wave number of incident wave P_1, whose subscript 1 indicates P_1 wave and subscript s represents the soil, and $\varphi_s = \theta_s + \theta_0 + \pi/2$. Time factor $\exp(-i\omega t)$ can be omitted due to all the excitation and response wave functions contain it.

For the sake of differentiating coupled scattering waves that emerged at cylindrical heterogeneity under incident P waves, scattering waves consisting of P_1, P_2, and SV wave are written as the series forms of displacement potential functions as follows:

$$ {}_{s}^{s}\phi_m^{sc} = \sum_{n=-\infty}^{+\infty} {}^{s}A_m H_n(\alpha_{1s} r_s)\, e^{in\theta_s}, \tag{2a} $$

$$ {}_{f}^{s}\phi_m^{sc} = \sum_{n=-\infty}^{+\infty} {}^{s}B_m H_n(\alpha_{2s} r_s)\, e^{in\theta_s}, \tag{2b} $$

$$ {}^{s}\psi_m^{sc} = \sum_{n=-\infty}^{+\infty} i\,{}^{s}C_m H_n(\beta_s r_s)\, e^{in\theta_s}, \tag{2c} $$

where the superscript sc on the right side of ϕ stands for scattering wave P; the subscripts s and f on the left side represent soil skeleton and fluid in soil medium, separately, which indicate the wave function of scattering wave P_1 and P_2; subscripts 1 and 2 of the wave number α indicate P_1 and P_2 wave too; ψ indicates the potential function of scattering SV wave; β_s is the wave number of scattering SV wave; A, B, and C represent the undetermined complex coefficients of scattering series expansion, respectively; subscript m means mth scattering; $H_n(\cdot)$ is the nth-order Hankel function of the first kind. The remaining symbols are the same as mentioned above.

2.2. Solution. The boundary conditions of the first order of scattering are

$$ \left[\sigma_{r_s r_s}^{\text{inc}}(r_s, \theta_s) + {}^{s}\sigma_{r_s r_s}^{1}(r_s, \theta_s)\right]\Big|_{r_s = a_s} = 0, \quad s = 0, 1, 2, \ldots, N,\ 0 \le \theta_s \le 2\pi, \tag{3a} $$

$$ \left[\sigma_{r_s \theta_s}^{\text{inc}}(r_s, \theta_s) + {}^{s}\sigma_{r_s \theta_s}^{1}(r_s, \theta_s)\right]\Big|_{r_s = a_s} = 0, \quad s = 0, 1, 2, \ldots, N,\ 0 \le \theta_s \le 2\pi. \tag{3b} $$

Assuming the cavity-soil interface is permeable, the fluid stress is free:

$$ \left[{}_{f}p^{\text{inc}}(r_s, \theta_s) + {}_{f}^{s}p^{1}(r_s, \theta_s)\right]\Big|_{r_s = a_s} = 0, \quad s = 0, 1, 2, \ldots, N,\ 0 \le \theta_s \le 2\pi, \tag{3c} $$

where all the superscripts 1 indicate the first scattering, the subscripts r and θ of soil skeleton stress σ represent radial and tangential stresses, and the letter p of fluid stress has the same definition as above.

Substituting the equilibrium equation of Biot's poroelastic theory under the cylindrical coordinate system, the stress of soil skeleton and fluid can be expressed by potential functions such as

$$ \begin{aligned} \sigma_{r_s r_s} = {} & \lambda\left(\frac{\partial^2 {}_{s}\phi}{\partial r_s^2} + \frac{1}{r_s}\frac{\partial {}_{s}\phi}{\partial r_s} + \frac{1}{r_s^2}\frac{\partial^2 {}_{s}\phi}{\partial \theta_s^2}\right) + 2G\left(\frac{\partial^2 \psi}{\partial r_s^2}\right. \\ & \left. + \frac{1}{r_s}\frac{\partial^2 \psi}{\partial r_s \partial \theta_s} - \frac{1}{r_s^2}\frac{\partial \psi}{\partial \theta_s}\right) + \eta M\left(\frac{\partial^2 {}_{f}\phi}{\partial r_s^2} + \frac{1}{r_s}\frac{\partial {}_{f}\phi}{\partial r_s}\right. \\ & \left. + \frac{1}{r_s^2}\frac{\partial^2 {}_{f}\phi}{\partial \theta_s^2}\right), \end{aligned} \tag{4a} $$

$$ \begin{aligned} \sigma_{r_s \theta_s} = {} & G\left(\frac{2}{r_s}\frac{\partial^2 {}_{s}\phi}{\partial r_s \partial \theta_s} - \frac{2}{r_s^2}\frac{\partial {}_{s}\phi}{\partial \theta_s} + \frac{1}{r_s^2}\frac{\partial^2 \psi}{\partial \theta_s^2} - \frac{\partial^2 \psi}{\partial r_s^2}\right. \\ & \left. + \frac{1}{r_s}\frac{\partial \psi}{\partial r_s}\right), \end{aligned} \tag{4b} $$

$$ \begin{aligned} -{}_{f}p = {} & M\left(\frac{\partial^2 {}_{f}\phi}{\partial r_s^2} + \frac{1}{r_s}\frac{\partial {}_{f}\phi}{\partial r_s} + \frac{1}{r_s^2}\frac{\partial^2 {}_{f}\phi}{\partial \theta_s^2}\right) + \eta M\left(\frac{\partial^2 {}_{s}\phi}{\partial r_s^2}\right. \\ & \left. + \frac{1}{r_s}\frac{\partial {}_{s}\phi}{\partial r_s} + \frac{1}{r_s^2}\frac{\partial^2 {}_{s}\phi}{\partial \theta_s^2}\right), \end{aligned} \tag{4c} $$

where λ and G are Lamé constant of soil skeleton, M indicates the compressibility constant of pore fluid, η indicates viscous coefficient of pore fluid, and the rest of the symbols' meanings are the same as before.

Substituting (1) and (4a), (4b), and (4c) into (3a), (3b), and (3c), there are

$$\begin{aligned}
&\lambda\left\{e^{i\alpha_{1s}r_{0s}(\theta_0+\theta_{0s})+in(\theta_0+\pi/2)}\sum_{n=-\infty}^{+\infty}\left[\alpha_{1s}^2J_n''(\alpha_{1s}a_s)\right.\right.\\
&\quad+\frac{\alpha_{1s}}{a_s}J_n'(\alpha_{1s}a_s)-\frac{n^2}{a_s^2}J_n(\alpha_{1s}a_s)\Big]\\
&\quad+\sum_{n=-\infty}^{+\infty}\left[\alpha_{1s}^2H_n''(\alpha_{1s}a_s)+\frac{\alpha_{1s}}{a_s}H_n'(\alpha_{1s}a_s)\right.\\
&\quad\left.\left.-\frac{n^2}{a_s^2}H_n(\alpha_{1s}a_s)\right]{}^sA_1\right\}+2G\sum_{n=-\infty}^{+\infty}i\left[\beta_s^2H_n''(\beta_sa_s)\right.\\
&\quad+\frac{in\beta_s}{a_s}H_n'(\beta_sa_s)-\frac{in}{a_s^2}H_n(\beta_sa_s)\Big]{}^sC_1\\
&\quad+\eta M\sum_{n=-\infty}^{+\infty}\left[\alpha_{2s}^2H_n''(\alpha_{2s}a_s)+\frac{\alpha_{2s}}{a_s}H_n'(\alpha_{2s}a_s)-\frac{n^2}{a_s^2}\right.\\
&\quad\left.\cdot H_n(\alpha_{2s}a_s)\right]{}^sB_1=0
\end{aligned}\tag{5a}$$

$$\begin{aligned}
&G\left\{e^{i\alpha_{1s}r_{0s}(\theta_0+\theta_{0s})+in(\theta_0+\pi/2)}\frac{2in}{a_s}\sum_{n=-\infty}^{+\infty}\left[\alpha_{1s}J_n'(\alpha_{1s}a_s)\right.\right.\\
&\quad\left.-\frac{1}{a_s}J_n(\alpha_{1s}a_s)\right]+\frac{2in}{a_s}\sum_{n=-\infty}^{+\infty}\left[\alpha_{1s}H_n'(\alpha_{1s}a_s)\right.\\
&\quad\left.-\frac{1}{a_s}H_n(\alpha_{1s}a_s)\right]{}^sA_1+i\sum_{n=-\infty}^{+\infty}\left[-\frac{n^2}{a_s^2}H_n(\beta_sa_s)\right.\\
&\quad\left.\left.-\beta_s^2H_n''(\beta_sa_s)+\frac{\beta_s}{a_s}H_n'(\beta_sa_s)\right]{}^sC_1\right\}=0
\end{aligned}\tag{5b}$$

$$\begin{aligned}
&M\sum_{n=-\infty}^{+\infty}\left[\alpha_{2s}^2H_n''(\alpha_{2s}a_s)+\frac{\alpha_{2s}}{a_s}H_n'(\alpha_{2s}a_s)-\frac{n^2}{a_s^2}\right.\\
&\quad\left.\cdot H_n(\alpha_{2s}a_s)\right]{}^sB_1\\
&\quad+\eta M\left\{e^{i\alpha_{1s}r_{0s}(\theta_0+\theta_{0s})+in(\theta_0+\pi/2)}\sum_{n=-\infty}^{+\infty}\left[\alpha_{1s}^2J_n''(\alpha_{1s}a_s)\right.\right.\\
&\quad+\frac{\alpha_{1s}}{a_s}J_n'(\alpha_{1s}a_s)-\frac{n^2}{a_s^2}J_n(\alpha_{1s}a_s)\Big]\\
&\quad+\sum_{n=-\infty}^{+\infty}\left[\alpha_{1s}^2H_n''(\alpha_{1s}a_s)+\frac{\alpha_{1s}}{a_s}H_n'(\alpha_{1s}a_s)\right.\\
&\quad\left.\left.-\frac{n^2}{a_s^2}H_n(\alpha_{1s}a_s)\right]{}^sA_1\right\}=0\\
&\qquad s=0,1,2,\ldots,N,\ 0\le\theta_s\le2\pi.
\end{aligned}\tag{5c}$$

Simplifying (5a), (5b), and (5c), the matrix equation $\mathbf{QX}=\mathbf{R}$ is obtained, where $\mathbf{Q}$ is a coefficients matrix, $\mathbf{X}$ is the first undetermined complex coefficients matrix of scattering (transmission), and $\mathbf{R}$ is a vector matrix, whose expression is as shown in the appendix. Subscripts of element q_{ij} and r_j are $i=1,2,\ldots,n$; $j=1,2,\ldots,m$, where $n=m=3$. Coefficients can be solved by means of Cramer's law, and the specific elements expressions of $\mathbf{Q}$ and $\mathbf{R}$ are shown in the appendix as well.

$$\sum_{n=-\infty}^{+\infty}\begin{bmatrix}q_{11}&q_{12}&q_{13}\\q_{21}&q_{22}&q_{23}\\q_{31}&q_{32}&q_{33}\end{bmatrix}\mathbf{X}=-{}^s\theta_\alpha\sum_{n=-\infty}^{+\infty}\begin{bmatrix}r_1\\r_2\\r_3\end{bmatrix},\tag{6}$$

where $\mathbf{X}=[{}^sA_1\quad{}^sB_1\quad{}^sC_1]^{\mathrm{T}}$, ${}^s\theta_\alpha=e^{i\alpha_{1s}r_{0s}(\theta_0+\theta_{0s})+in(\theta_0+\pi/2)}$.

For the mth ($m\ge2$) order of scattering, the first order of scattering waves is all regarded as the origin of secondary wave, and the stress boundary conditions at interface are satisfied with those

$$\left[{}^s\sigma_{r_sr_s}^m(r_s,\theta_s)+\sum_{s'=0,s'\ne s}^{N'}{}'{}^{s'}\sigma_{r_{s'}r_{s'}}^{m-1}(r_{s'},\theta_{s'})\right]\Bigg|_{r_s=a_s}=0,\tag{7a}$$

$$s=0,1,2,\ldots,N,\ 0\le\theta_s\le2\pi,\ m\ge2,$$

$$\left[{}^s\sigma_{r_s\theta_s}^m(r_s,\theta_s)+\sum_{s'=0,s'\ne s}^{N'}{}'{}^{s'}\sigma_{r_{s'}\theta_{s'}}^{m-1}(r_{s'},\theta_{s'})\right]\Bigg|_{r_s=a_s}=0,\tag{7b}$$

$$s=0,1,2,\ldots,N,\ 0\le\theta_s\le2\pi,\ m\ge2.$$

The fluid at interface also meets the stress-free condition as follows:

$$\left[{}_{\mathrm{f}}p^{\mathrm{inc}}(r_s,\theta_s)+\sum_{s'=0,s'\ne s}^{N'}{}'{}_{\mathrm{f}}^{s'}p^{m-1}(r_{s'},\theta_{s'})\right]\Bigg|_{r_s=a_s}=0,\tag{7c}$$

$$s=0,1,2,\ldots,N,\ 0\le\theta_s\le2\pi,\ m\ge2.$$

As the coordinates depicted above, it is required to transfer the origin of the elementary wave functions so as to implement the boundary conditions.

Therefore, the iterative relation of the mth ($m\ge2$) order of scattering coefficients is $\mathbf{QX}=\mathbf{SY}$, where $\mathbf{Q}$ is defined as the same expression before, $\mathbf{X}$ is the mth-order of scattering coefficients, $\mathbf{Y}$ is the complex coefficients matrix obtained previously, and $\mathbf{S}$ is the vector matrix; thus the expression matrix can be reached as

$$\begin{aligned}
&\sum_{n=-\infty}^{+\infty}\begin{bmatrix}q_{11}&q_{12}&q_{13}\\q_{21}&q_{22}&q_{23}\\q_{31}&q_{32}&q_{33}\end{bmatrix}\mathbf{X}\\
&\quad=-\sum_{s'=0,s'\ne s}^{N'}{}'\sum_{n'=-\infty}^{+\infty}\sum_{n=-\infty}^{+\infty}\begin{bmatrix}s_{11}&s_{12}&s_{13}\\s_{21}&s_{22}&s_{23}\\s_{31}&s_{32}&s_{33}\end{bmatrix}\mathbf{Y},
\end{aligned}\tag{8}$$

where $\mathbf{X}=[{}^sA_m\quad{}^sB_m\quad{}^sC_m]^{\mathrm{T}}$, $\mathbf{Y}=[{}^{s'}A_{m-1}\quad{}^{s'}B_{m-1}\quad{}^{s'}C_{m-1}]^{\mathrm{T}}$, and the specific elements expressions of $\mathbf{S}$ are also stated in the appendix. Reference coordinates transformation is manipulated by means of Graf's additional theorem.

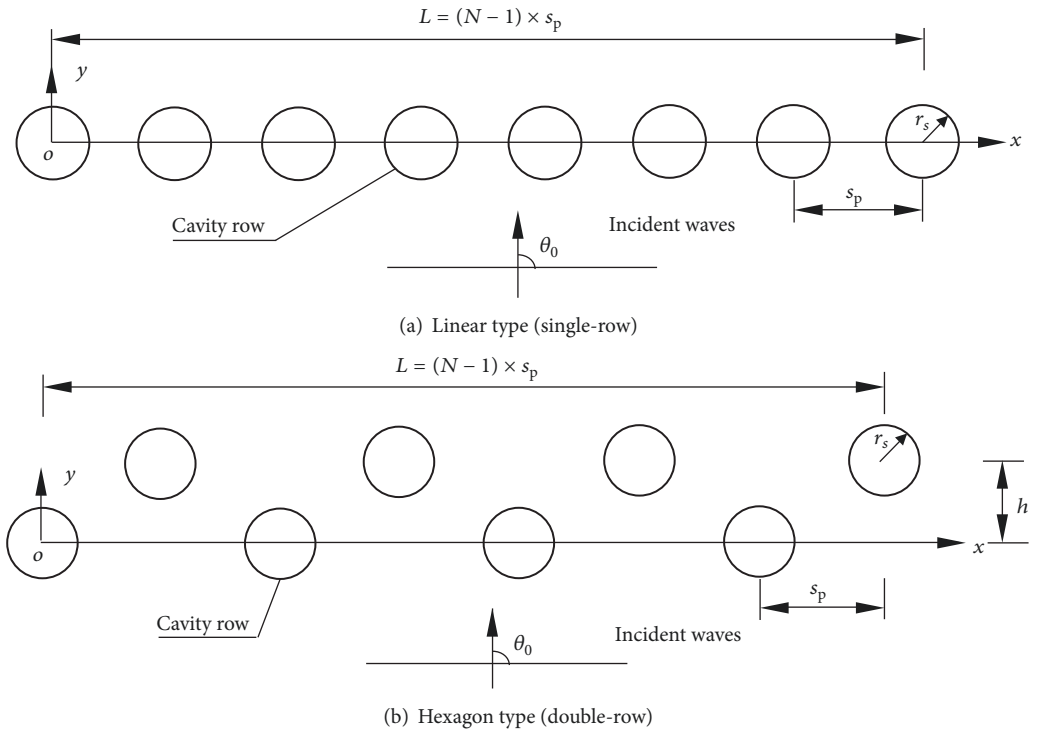

Figure 4: Calculation model of equally spaced and unidiameter parallel cavity barriers in saturated soil.

3. Numerical Example Analyses

Assuming that the surrounding soil is a homogenous and saturated medium and the depth of cavity is infinite, it turns out to be a total space two-phase problem. There is a series of time-harmonic plane P_1 waves propagating perpendicularly to the group of cavities. The angle of incident P_1 wave is $\theta_0 = \pi/2$. The cross-section shapes of all the cavities are all round, with the identical radius $r_s = a_s$. The length of the barrier is L, and all the neighboring cavities are uniformly spaced with the spacing S_p (from center of one cavity to the center of the contiguous one). In order to compare between the numerical examples of Avilés and Sánchez-Sesma [2], N-cavity ($N = 8$) barrier with two configurations, linear (single-row) and hexagon (double-row), is illustrated in Figure 4. The origin o of the coordinate is at the center of the very left cavity.

When the barrier is hexagonally arranged, it becomes a double-row barrier, and the row-distance is h; when $h = 0$, it is degenerated to a linear arrangement as Figure 4(a). The Bessel function truncated terms n should be no less than 8 so that the numerical accuracy would be guaranteed [27].

The selected soil physical and mechanical parameters are listed in Table 1 [4].

The incident wave frequency is treated as dimensionless while doing numerical calculation:

$$\zeta_{ps} = \frac{2a_s}{\Lambda_{ps}} = \frac{\alpha_{1s}a_s}{\pi} \tag{9a}$$

$$\zeta_{pf} = \frac{2a_s}{\Lambda_{pf}} = \frac{\alpha_{2s}a_s}{\pi} \tag{9b}$$

$$\zeta_{ss} = \frac{2a_s}{\Lambda_{ss}} = \frac{\beta_s a_s}{\pi}, \tag{9c}$$

where ζ indicates dimensionless frequency, Λ indicates wavelength, superscripts are the same as above, and the wave numbers refer to literature [4]. The absolute value of dimensionless displacement amplitude $|u/u_0|$ represents the ratio of total scattering P wave displacement amplitude and the incident wave displacement amplitude.

The influences of scattering order, cavity spacing, row-distance, and configuration of arrangement are discussed as below.

3.1. Model Verification. On one hand, a comparison with the existing theoretical result [11] in elastic media is carried out in Figure 5(a), where the dash curve demonstrates the midline dimensionless displacement amplitude $|u/u_0|$ behind the single-row piles encountering a series of incident P waves, with inner radius b_s is 0 (degenerated to cavities, SD = 5); meanwhile the solid line is with the present method in single-phased elastic soil when $m = 1$. A good agreement between the two curves which validates the accuracy of the present solution is obviously seen.

On the other hand, the variation curves of midline dimensionless displacement amplitude behind the single-row cavity barrier when scattering orders m varies from 1 to 5 are depicted. It can be observed that the similar variation trend compared with reference [26], which presents amplitude amplification phenomenon at a certain range near the barrier ($0 \le y/a_s \le 50$); following a sharp attenuation, the displacement amplitude decreases to about 0.5. With

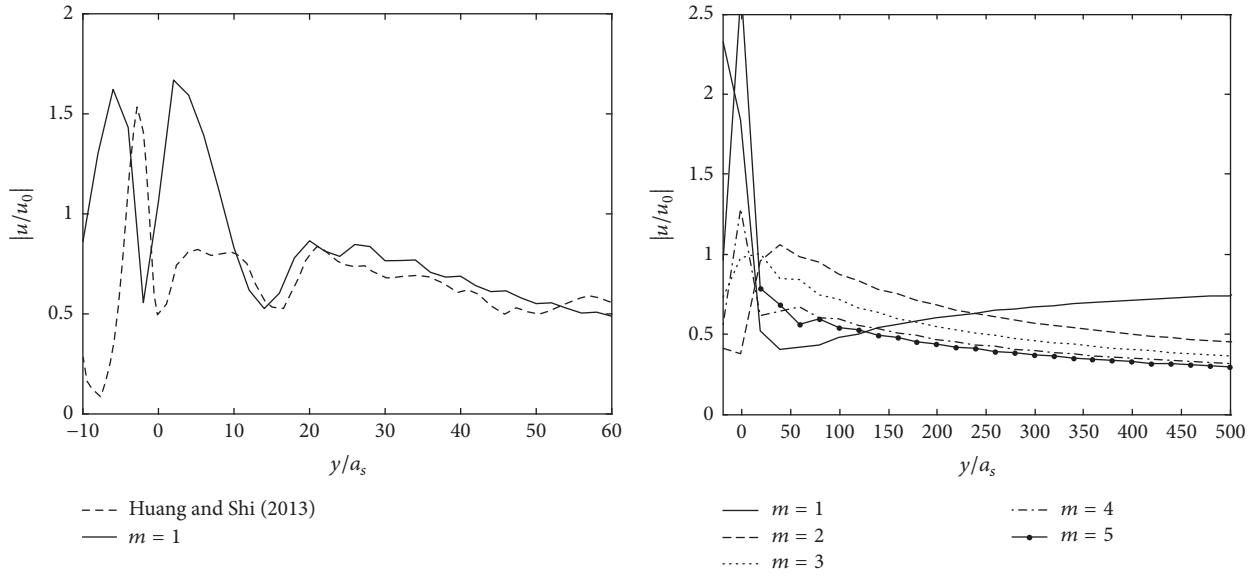

(a) In elastic media

(b) In saturated soil ($1 \le m \le 5$)

FIGURE 5: Midline dimensionless displacement amplitude $|u/u_0|$ behind the single-row cavity barrier with variation of scattering orders in saturated soil ($s_p/a_s = 3.0$).

TABLE 1: Biot's parameters in saturated soil.

λ (Gpa)	G (10^{-2} Pa)	ρ_f (kg/m^3)	η	M (Gpa)	ρ_1 (kg/m^3)	ζ_{ps}	ζ_{pf}	ζ_{ss}
7.556	2.61	1000	0.94	7.407	2204.5	0.45	0.8	0.6

λ and G are Lamé constant of the soil, ρ_f stands for the mass density of fluid, η is the coefficient of fluid compression, M is the constant of compressibility in soil, and ρ_1 stands for the mass density of soil.

the increase of the scattering order m, $|u/u_0|$ is decreasing gradually, and the increment is attenuating, with a trend of convergence, especially when scattering order m values 4 to 5' there are few differences between the numerical calculation results. It is indicated that the multiple scattering assumption is credible and a numerical truncation at $m = 4$ is acceptable when it comes to design a cavity barrier. Secondly, the displacement amplitude behind the barrier at a certain distance ($y/a_s > 250$) reaches 0.75 under the single order of scattering hypothesis, which achieves 1.5-time value of the results under the double order of scattering ($m = 2$) hypothesis. A fact that the displacement amplitude increment will be enlarged more than 50% is depicted when using single scattering hypothesis, which no doubt leads to increasing the safety of barrier design. In other words, more material of barrier will result in waste, which cannot be ignored in barrier design.

3.2. Screening Effectiveness Influenced by the Variation of Position behind the Barrier. The property of displacement amplitude $|u/u_0|$ with different position behind the barrier is illustrated in Figure 6. When the separation between single-row cavities ($h = 0.0a_s$) is $s_p = 2.5a_s$ (Figure 6(a)), with the variation of position (from the midline $x/a_s = 7.5$ to the margin of the barrier, $x/a_s = 15.0$), $|u/u_0|$ occurs to attenuate with a similar trend, which can be observed at the following contour map as well. Regardless of the amplitude amplification phenomenon or the attenuation value at the near range of barrier, there is subtle distinction from the midline $x/a_s = 7.5$ to $x/a_s = 12.5$, which manifests that selecting a reasonable separation of cavities leads to a homogeneous isolated expression until at a further distance of $x/a_s = 15.0$, $|u/u_0|$ performs increasing. It indicates a parallel characteristics at a double-row barrier when the distance is $h = 2.5a_s$. The curves group shows a bigger amplification near the barrier and a faster attenuation along the different positions behind the barrier at the same time, which demonstrates the double-row barrier will present as a much continuous property of isolation vibration. The detailed result is referred to Section 3.4.

3.3. Screening Effectiveness Influenced by the Variation of Cavity Spacing. The contour of dimensionless displacement amplitude $|u/u_0|$ with the variation of cavity spacing in Figure 7 is shown. Amplification of dimensionless displacement amplitude at the central region behind the barrier is obviously observed ($0 \le y/a_s \le 150$). The displacement amplitude attenuates radially with the increasing of cavity spacing. No less than 40% incident waves are isolated at most area behind the barrier ($150 \le y/a_s \le 400$). Secondly, with the increase of the cavity spacing ($2.5 \le s_p/a_s \le 4.0$), the screening effectiveness decreases gradually, which the

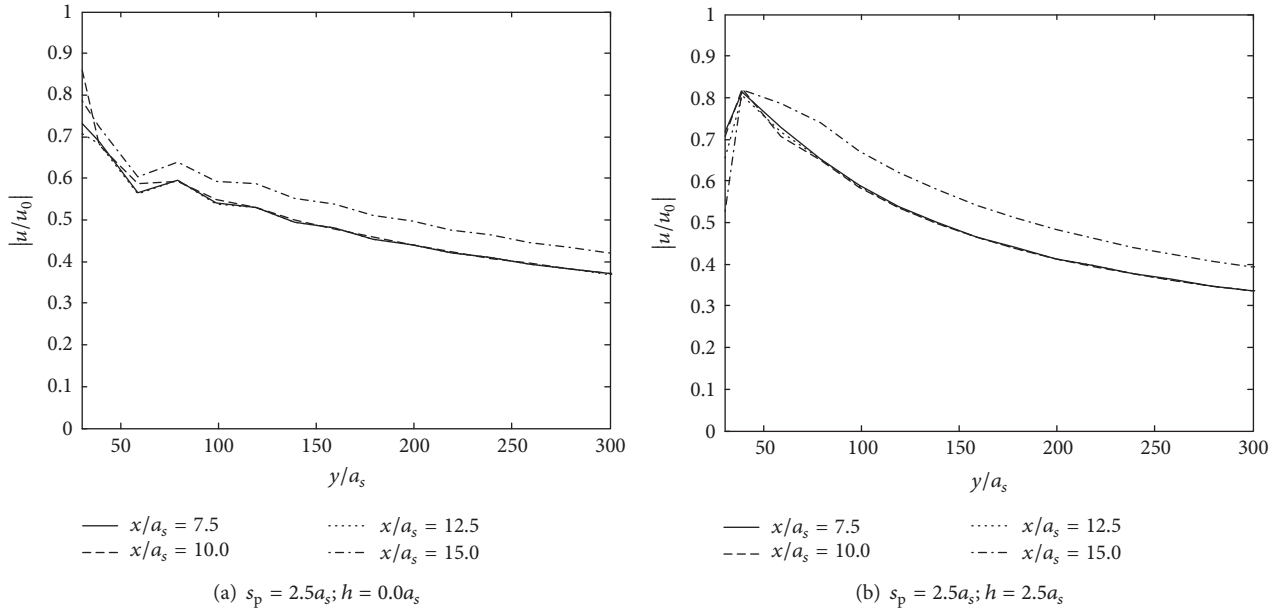

(a) $s_p = 2.5a_s$; $h = 0.0a_s$ (b) $s_p = 2.5a_s$; $h = 2.5a_s$

FIGURE 6: Dimensionless displacement amplitude $|u/u_0|$ with the variation of position behind the cavity barrier via y/a_s-axis ($m = 4$).

optimum isolation region is away from the barrier. This is owing to the fact that increase of cavity spacing leads to increase the probability of incident wave transmission and diffraction against the barrier. Thus the dimensionless cavity spacing s_p/a_s usually can be designed between 2.5 and 3.0.

3.4. Screening Effectiveness Influenced by the Variation of Row-Distance. Figure 8 depicts a series of displacement amplitude $|u/u_0|$ contour variation with row-distance changing. For the sake of comparison with single-row cavity barrier in Figure 7(a), $s_p/a_s = 2.5$ is adopted in all Figure 8 as two-row cavity barrier. It is presented that the optimum range is more closer to barrier in double-row barrier (Figure 8(a)) than that in single-row barrier (Figure 7(a)). The range that can shield off 60% incident wave is carried forward from $y/a_s =$ 350 to 200. Therefore increasing the row-distance leads to significant improvement of isolated effect on the premise of same cavity numbers, which exactly thickens the barrier and rearranges the cavity rows. Secondly, the difference between enlarging the cavity spacing and row-distance is that the latter one will significantly enhance the isolated effect; until the row-distance rises to $s_p/a_s = 4.0$ in Figure 8(a), the dimensionless displacement amplitude $|u/u_0|$ will gradually increase; Therefore, the multirow cavity barrier will achieve a better vibration isolation effect when it is designed with a certain range ($2.5 \leq h/a_s \leq 3.5$) of row-distance in calculation.

3.5. Screening Effectiveness Influenced by the Variation of Barrier Arrangement and Cavity Number. In order to investigate the multiple scattering properties and characteristics of elastic waves by cavity rows as barrier with different arrangement in in saturated soil, a double-row rectangular arrangement (counterpoint) is implemented in Figure 9 to compare with the rows in hexagonal-shaped as mentioned above. Figure 10 illustrates a $5.0a_s$ catity-spacing and $2.5a_s$ row-distance two-row barrier. Compared with the displacement amplitude in Figure 8(a) in hexagonal arrangement, Figure 10 performs a weaker screening ability of elastic P waves, which at the most of the region ($0 \leq y/a_s \leq 500$) could only approach 20% isolated effectiveness. It is inferred that although the calculation distances seem identical, rectangular-shaped barrier actually widens the spacing of the barrier, which brings about more incident waves passing through the cavity rows and spreads them behind the barrier, so that it does not play a preferable role of isolation. As a consequence, the counterchanged-shaped double-row barrier is usually considered as an ideal arrangement in practical engineering, namely, hexagonal arrangement.

On the other hand, the influence of screening effectiveness with the variation of cavity number is also significant. Midline displacement amplitude behind the barrier with different number of cavities is showed in Figure 11. Increase of cavity number results in a superior isolated effectiveness. When doubling the cavity number, the decrement of displacement amplitude will reduce to 50%. It is manifested that increase of the cavity number is amount to widening the barrier when the cavity spacing is identical.

4. Concluding Remarks

Based on the Biot's poroelastic theory and multiple scattering theory, the plane P_1 waves' multiple scattering by arbitrarily arranged and arbitrary radius cavity barrier in saturated soil is derived and solved. The screening effectiveness of P_1 waves by single and multirow cavities has been calculated in numerical analysis, which concludes that

(1) Multiple scattering assumption compensates the defects of ignoring the wave coherent phenomenon of subsequent scattering in former analysis for it regarding the

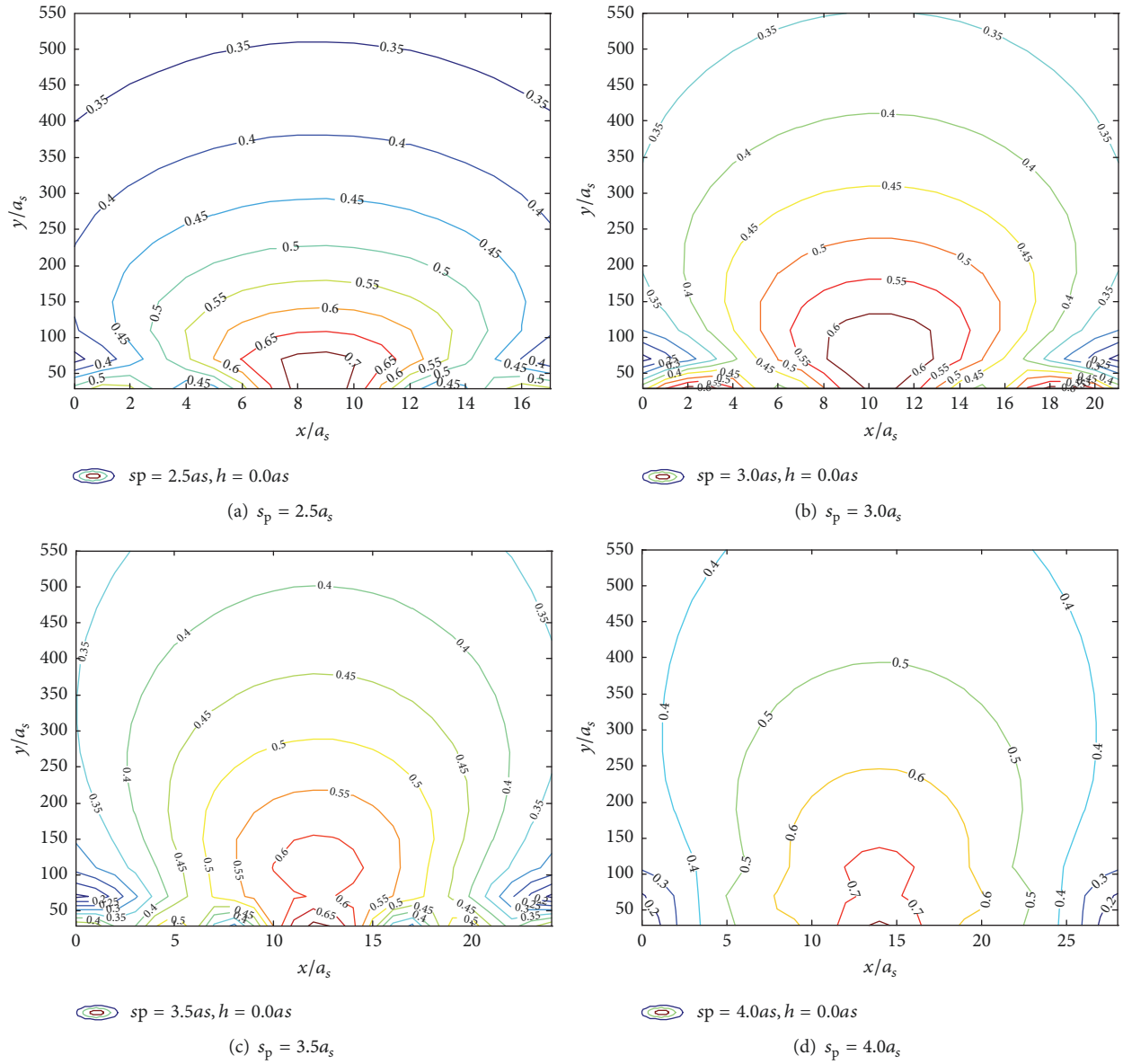

FIGURE 7: Dimensionless displacement amplitude $|u/u_0|$ contour behind the single-row cavity barrier with variation of separation in saturated soil ($m = 4$).

scattering wave as a secondary wave source. Numerical results indicate that the displacement amplitudes behind the barrier are much less with the multiple scattering assumption than considering single scattering only. Therefore, the deviation caused by subsequent scattering cannot be neglected in the vibration isolation design. As the order of scattering increases, the displacement amplitude tends to converge; it will obtain higher calculation accuracy when the order of scattering is truncated at $m = 4$.

(2) Increase of the cavity spacing will decrease the isolation effectiveness of the barrier, and the optimum range also presents far away from the barrier; that is, the result of increase of the cavity spacing leading to more transmission and diffraction of incident waves. Increasing the row-distance could also improve the isolated effect when the total numbers of cavities are equal. It is resulted from increase of row-distance giving rise to thicken the barrier. The screening effect declines when row-distance increases to a certain distance at $s_p/a_s = 4.0$; it is considered to select $2.5 \le s_p/a_s \le 3.0$, and $2.5 \le h/a_s \le 3.5$ while designing of cavity spacing and row-distance, respectively.

(3) The scattering characteristics of cavity rows with various arrangement are different. The isolation properties of elastic waves with rectangular arrangement (counterpoint) are weaker than that with hexagonal arrangement (counterchanged) when the row-distance of barrier is uniform. Rectangular arrangement actually widens the cavity spacing, which makes more incident waves to be diffracted behind the barrier. Thus hexagonal arrangement is usually used in practical engineering. The screening effectiveness influenced

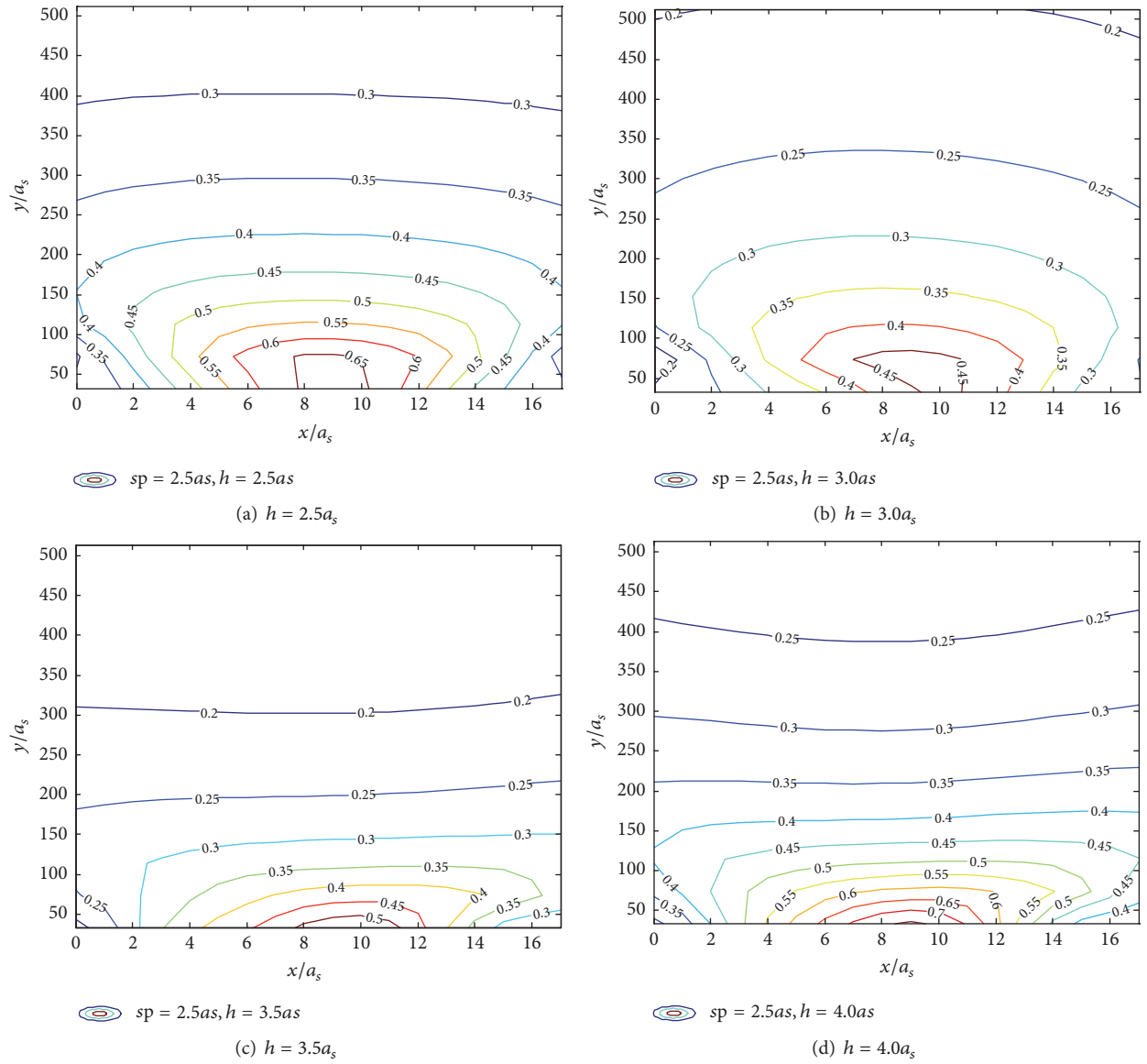

Figure 8: Dimensionless displacement amplitude $|u/u_0|$ contour behind the double-row cavity barrier with variation of distance in saturated soil ($m = 4$; $s_p = 2.5a_s$).

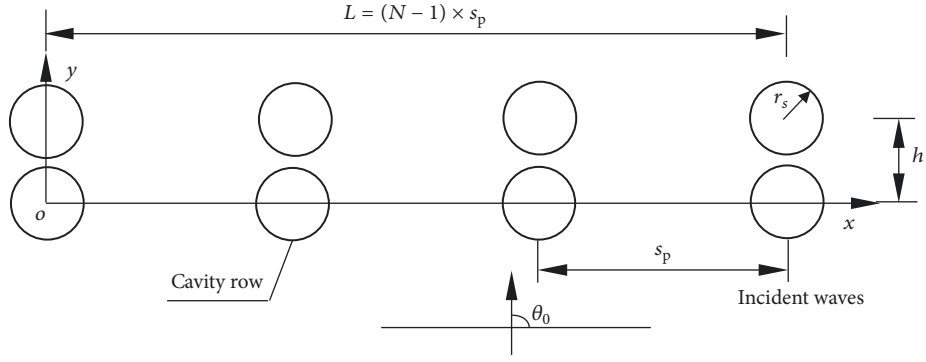

Figure 9: Calculation model of equally spaced and unidiameter parallel cavity barrier in saturated soil (counterpoint). Hexagon type.

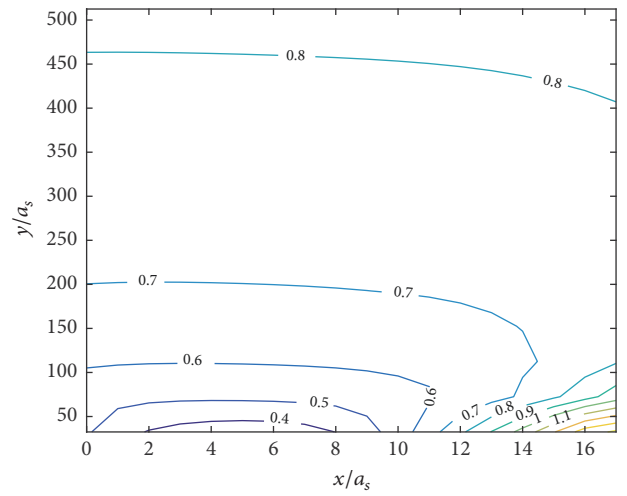

Figure 10: Dimensionless displacement amplitude $|u/u_0|$ contour behind the double-row cavity barrier rectangularly arranged in saturated soil ($m = 4$; $h = 2.5a_s$).

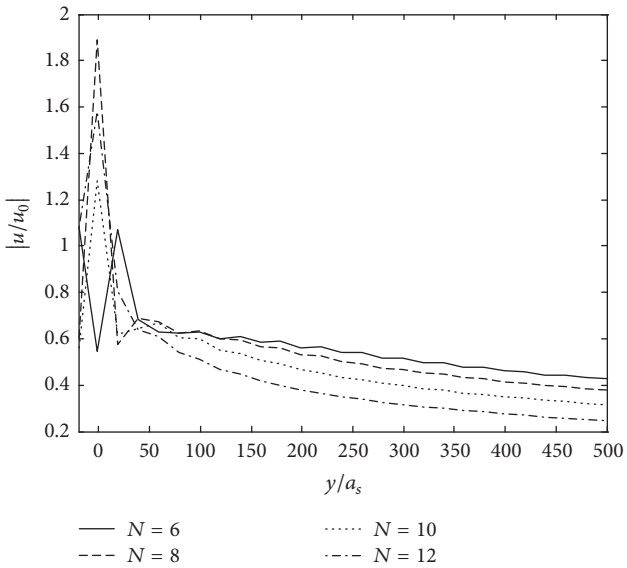

Figure 11: Midline dimensionless displacement amplitude $|u/u_0|$ behind the single-row cavity barrier with variation of cavity number in saturated soil ($m = 4$; $h = 2.5a_s$).

by cavity number is also remarkable, and with the number increases, the barrier widens, so that the isolation effect is improved as well.

Appendix

Symbolic Meaning

$$q_{11} = \lambda \left[\alpha_{1s}^2 H_n'' (\alpha_{1s} a_s) + \frac{\alpha_{1s}}{a_s} \cdot H_n' (\alpha_{1s} a_s) - \frac{n^2}{a_s^2} \cdot H_n (\alpha_{1s} a_s) \right];$$

$$q_{12} = \eta M \left[\alpha_{2s}^2 H_n'' (\alpha_{2s} a_s) + \frac{\alpha_{2s}}{a_s} \cdot H_n' (\alpha_{2s} a_s) - \frac{n^2}{a_s^2} \cdot H_n (\alpha_{2s} a_s) \right];$$

$$q_{13} = 2G \left[i\beta_s^2 H_n'' (\beta_s a_s) - \frac{n\beta_s}{a_s} \cdot H_n' (\beta_s a_s) + \frac{n}{a_s^2} \cdot H_n (\beta_s a_s) \right];$$

$$q_{21} = 2inG \left[\frac{\alpha_{1s}}{a_s} \cdot H_n' (\alpha_{1s} a_s) - \frac{1}{a_s^2} \cdot H_n (\alpha_{1s} a_s) \right];$$

$$q_{22} = 0;$$

$$q_{23} = iG \left[-\frac{n^2}{a_s^2} \cdot H_n (\beta_s a_s) - \beta_s^2 H_n'' (\beta_s a_s) + \frac{\beta_s}{a_s} \cdot H_n' (\beta_s a_s) \right];$$

$$q_{31} = \eta M \left[\alpha_{1s}^2 H_n'' (\alpha_{1s} a_s) + \frac{\alpha_{1s}}{a_s} \cdot H_n' (\alpha_{1s} a_s) - \frac{n^2}{a_s^2} \cdot H_n (\alpha_{1s} a_s) \right];$$

$$q_{32} = M \left[\alpha_{2s}^2 H_n'' (\alpha_{2s} a_s) + \frac{\alpha_{2s}}{a_s} \cdot H_n' (\alpha_{2s} a_s) - \frac{n^2}{a_s^2} \cdot H_n (\alpha_{2s} a_s) \right];$$

$$q_{33} = 0;$$

$$r_1 = \lambda \left[\alpha_{1s}^2 J_n'' (\alpha_{1s} a_s) + \frac{\alpha_{1s}}{a_s} \cdot J_n' (\alpha_{1s} a_s) - \frac{n^2}{a_s^2} \cdot J_n (\alpha_{1s} a_s) \right];$$

$$r_2 = 2inG \left[\frac{\alpha_{1s}}{a_s} \cdot J_n' (\alpha_{1s} a_s) - \frac{1}{a_s^2} \cdot J_n (\alpha_{1s} a_s) \right];$$

$$r_3 = \eta M \left[\alpha_{1s}^2 J_n'' (\alpha_{1s} a_s) + \frac{\alpha_{1s}}{a_s} \cdot J_n' (\alpha_{1s} a_s) - \frac{n^2}{a_s^2} \cdot J_n (\alpha_{1s} a_s) \right];$$

$$s_{11} = \lambda \left[\alpha_{1s}^2 {}^s\mathscr{H}_{n'n} (\alpha_{1s} a_{ss'}) J_n'' (\alpha_{1s} a_s) + \frac{\alpha_{1s}}{a_{s'}} \cdot {}^s\mathscr{H}_{n'n} (\alpha_{1s} a_{ss'}) J_n' (\alpha_{1s} a_s) - \frac{n'^2}{a_{s'}^2} \cdot {}^s\mathscr{H}_{n'n} (\alpha_{1s} a_{ss'}) J_n (\alpha_{1s} a_s) \right];$$

$$
\begin{aligned}
s_{12} &= \eta M \left[\alpha_{2s}^2 \, {}^{s}\mathscr{H}_{n'n}(\alpha_{2s} a_{ss'}) \, J_n''(\alpha_{2s} a_s) + \frac{\alpha_{2s}}{a_{s'}} \right. \\
&\quad \cdot {}^{s}\mathscr{H}_{n'n}(\alpha_{2s} a_{ss'}) \, J_n'(\alpha_{2s} a_s) - \frac{n'^2}{a_{s'}^2} \\
&\quad \left. \cdot {}^{s}\mathscr{H}_{n'n}(\alpha_{2s} a_{ss'}) \, J_n(\alpha_{2s} a_s) \right]; \\
s_{13} &= 2G \left[i\beta_s^{2s} \mathscr{H}_{n'n}(\beta_s a_{ss'}) \, J_n''(\beta_s a_s) - \frac{n' \beta_s}{a_{s'}} \right. \\
&\quad \cdot {}^{s}\mathscr{H}_{n'n}(\beta_s a_{ss'}) \, J_n'(\beta_s a_s) + \frac{n'}{a_{s'}^2} \\
&\quad \left. \cdot {}^{s}\mathscr{H}_{n'n}(\beta_s a_{ss'}) \, J_n(\beta_s a_s) \right]; \\
s_{21} &= \frac{2in'G}{a_{s'}} \left[\alpha_{1s} \mathscr{H}_{n'n}(\alpha_{1s} a_{ss'}) \, J_n'(\alpha_{1s} a_s) \right. \\
&\quad \left. - \frac{1}{a_{s'}} \mathscr{H}_{n'n}(\alpha_{1s} a_{ss'}) \, J_n(\alpha_{1s} a_s) \right]; \\
s_{22} &= 0; \\
s_{23} &= iG \left[-\frac{n'^2}{a_{s'}^2} \cdot \mathscr{H}_{n'n}(\beta_s a_{ss'}) \, J_n(\beta_s a_s) \right. \\
&\quad - \beta_s^2 \mathscr{H}_{n'n}(\beta_s a_{ss'}) \, J_n''(\beta_s a_s) + \frac{\beta_s}{a_{s'}} \\
&\quad \left. \cdot {}^{s}\mathscr{H}_{n'n}(\beta_s a_{ss'}) \, J_n'(\beta_s a_s) \right]; \\
s_{31} &= \eta M \left[\alpha_{1s}^2 H_n''(\alpha_{1s} a_s) + \frac{\alpha_{1s}}{a_s} \cdot H_n'(\alpha_{1s} a_s) - \frac{n^2}{a_s^2} \right. \\
&\quad \left. \cdot H_n(\alpha_{1s} a_s) \right]; \\
s_{32} &= M \left[\alpha_{2s}^2 \, {}^{s}\mathscr{H}_{n'n}(\alpha_{2s} a_{ss'}) \, J_n''(\alpha_{2s} a_s) + \frac{\alpha_{2s}}{a_{s'}} \right. \\
&\quad \cdot {}^{s}\mathscr{H}_{n'n}(\alpha_{2s} a_{ss'}) \, J_n'(\alpha_{2s} a_s) - \frac{n'^2}{a_{s'}^2} \\
&\quad \left. \cdot {}^{s}\mathscr{H}_{n'n}(\alpha_{2s} a_{ss'}) \, J_n(\alpha_{2s} a_s) \right]; \\
s_{33} &= 0,
\end{aligned}
\tag{A.1}
$$

where $H_{n'}(\omega r_{s'}) e^{in'\theta_{s'}} = \sum_{n'=-\infty}^{+\infty} \sum_{n=-\infty}^{+\infty} H_{n-n'}(\omega r_{ss'}) J_n(\omega r_s) \cdot e^{in\theta_s - i(n-n')\theta_{ss'}}$, ${}^{s}\mathscr{H}_{n'n}(\cdot) = H_{n-n'}(\cdot) e^{-i(n-n')\theta_{ss'}}$.

The variable ω represents the wave P or the wave SV number.

Conflicts of Interest

The authors declare that they have no conflicts of interest.

Acknowledgments

The work described in this paper was supported by the National Natural Science Foundation of China (Grant no. 51408549) and Zhejiang Provincial Natural Science Foundation of China (Grant nos. LY18E080024, LY16E090005, and LQ15E080008).

References

[1] Y. Pao, C. Mow, and J. D. Achenbach, "Diffraction of Elastic Waves and Dynamic Stress Concentrations," *Journal of Applied Mechanics*, vol. 40, no. 4, p. 872, 1973.

[2] J. Avilés and F. J. Sánchez-Sesma, "Piles as barriers for elastic waves," *Journal of Geotechnical Engineering*, vol. 109, no. 9, pp. 1133–1146, 1983.

[3] J. Avilés and F. J. Sánchez-Sesma, "Foundation isolation from vibrations using piles as barriers," *Journal of Engineering Mechanics*, vol. 114, no. 11, pp. 1854–1870, 1988.

[4] Y. Hu, L. Z. Wang, Y. M. Chen, S. Wu M, and M. Z. Zhang, "scattering and refraction of plain strain waves at cylinders in saturated soil," *Acta Seismologica sinica*, vol. 20, no. 3, pp. 300–307, 1998.

[5] S. Liao and D. A. Sangrey, "Use of piles as isolation barriers," *Journal of the Geotechnical Engineering division*, vol. 104, no. 9, pp. 1139–1152, 1978.

[6] S. E. Kattis, D. Polyzos, and D. E. Beskos, "Vibration isolation by a row of piles using a 3-D frequency domain BEM," *International Journal for Numerical Methods in Engineering*, vol. 46, no. 5, pp. 713–728, 1999.

[7] P. Tsai, Z. Feng, and T. Jen, "Three-dimensional analysis of the screening effectiveness of hollow pile barriers for foundation-induced vertical vibration," *Computers & Geosciences*, vol. 35, no. 3, pp. 489–499, 2008.

[8] P. Xu, Y. Tie, and B. Chen, "Isolation of fast longitudinal waves by barriers composed of several rows of cylindrical cavities in saturated soils," *Zhendong yu Chongji*, vol. 34, no. 16, pp. 73–78, 2015.

[9] J.-F. Lu, B. Xu, and J.-H. Wang, "Numerical analysis of isolation of the vibration due to moving loads using pile rows," *Journal of Sound and Vibration*, vol. 319, no. 3-5, pp. 940–962, 2009.

[10] J.-F. Lu, X. Zhang, and R. Zhang, "A wavenumber domain boundary element model for the vibration isolation via a new type of pile structure: Linked pile rows," *Archive of Applied Mechanics*, vol. 84, no. 3, pp. 401–420, 2014.

[11] J. Huang and Z. Shi, "Application of periodic theory to rows of piles for horizontal vibration attenuation," *International Journal of Geomechanics*, vol. 13, no. 2, pp. 132–142, 2013.

[12] J. Huang and Z. Shi, "Attenuation zones of periodic pile barriers and its application in vibration reduction for plane waves," *Journal of Sound and Vibration*, vol. 332, no. 19, pp. 4423–4439, 2013.

[13] J. Huang and Z. Shi, "Vibration reduction of plane waves using periodic in-filled pile barriers," *Journal of Geotechnical and Geoenvironmental Engineering*, vol. 141, no. 6, Article ID 04015018, 2015.

[14] X. Zhang and J.-F. Lu, "A wavenumber domain boundary element method model for the simulation of vibration isolation by periodic pile rows," *Engineering Analysis with Boundary Elements*, vol. 37, no. 7-8, pp. 1059–1073, 2013.

[15] G. Carta, A. B. Movchan, L. P. Argani, and O. S. Bursi, "Quasi-periodicity and multi-scale resonators for the reduction of seismic vibrations in fluid-solid systems," *International Journal of Engineering Science*, vol. 109, pp. 216–239, 2016.

[16] A. Turan, D. Hafez, and M. H. El Naggar, "The performance of inclined secant micro-pile walls as active vibration barriers," *Soil Dynamics and Earthquake Engineering*, vol. 55, pp. 225–232, 2013.

[17] Y.-Q. Cai, G.-Y. Ding, and C.-J. Xu, "Amplitude reduction of elastic waves by a row of piles in poroelastic soil," *Computers & Geosciences*, vol. 36, no. 3, pp. 463–473, 2009.

[18] Y. Cai, G. Ding, C. Xu, and J. Wang, "Vertical amplitude reduction of Rayleigh waves by a row of piles in a poroelastic half-space," *International Journal for Numerical and Analytical Methods in Geomechanics*, vol. 33, no. 16, pp. 1799–1821, 2009.

[19] P. Xu and T. Xia, "Analysis of isolation effects of P1 waves by barriers composed of a row of hollow pipe piles in saturated soils," *Tumu Gongcheng Xuebao/China Civil Engineering Journal*, vol. 46, no. 2, pp. 152–157, 2013.

[20] R. D. Woods, N. E. Barnett, and R. Sagesser, "A new tool for soil dynamics," *Journal of Geotechnical Engineering Division*, vol. 100, no. 11, pp. 1231–1247, 1974.

[21] P. Xu, D. T. Xia, and X. M. Zhou, "Elastic wave scattering by a cylinder in saturated soils," *Bulletin of science and technology*, vol. 22, no. 6, pp. 802–812, 2006.

[22] V. Twersky, "Multiple Scattering of Radiation by an Arbitrary Configuration of Parallel Cylinders," *The Journal of the Acoustical Society of America*, vol. 24, no. 1, pp. 42–46, 1952.

[23] V. Twersky, "Multiple scattering of radiation by an arbitrary planar configuration of parallel cylinders and by two parallel cylinders," *Journal of Applied Physics*, vol. 23, no. 4, pp. 407–414, 1952.

[24] S. Sancar and Y.-H. Pao, "Spectral analysis of elastic pulses backscattered from two cylindrical cavities in a solid. Part I," *The Journal of the Acoustical Society of America*, vol. 69, no. 6, pp. 1591–1596, 1981.

[25] S. Sancar and W. Sachse, "Spectral analysis of elastic pulses backscattered from two cylindrical cavities in a solid. Part II," *The Journal of the Acoustical Society of America*, vol. 69, no. 6, pp. 1597–1609, 1981.

[26] T.-D. Xia, M.-M. Sun, C. Chen, W.-Y. Chen, and X. Ping, "Analysis on multiple scattering by an arbitrary configuration of piles as barriers for vibration isolation," *Soil Dynamics and Earthquake Engineering*, vol. 31, no. 3, pp. 535–545, 2011.

[27] M.-M. Sun, G.-Q. Liang, T.-D. Xia et al., "Ground vibration isolation of multiple scattering by using rows of tubular piles as barriers," *Shock and Vibration*, vol. 2014, Article ID 894213, 2014.

[28] M. A. Biot, "Theory of propagation of elastic waves in a fluid-saturated porous solid. I. Low-frequency range," *The Journal of the Acoustical Society of America*, vol. 28, pp. 168–178, 1956.

[29] M. A. Biot, "Theory of propagation of elastic waves in a fluid-saturated porous solid. II. Higher frequency range," *The Journal of the Acoustical Society of America*, vol. 28, pp. 179–191, 1956.

[30] A. J. Fhilippacopoulos, "Waves in partially saturated medium due to surface loads," *Journal of Engineering Mechanics*, vol. 114, no. 10, pp. 1740–1759, 1988.